Nuclear Instruments and Methods in Physics Research A292 (1990) 329–336
North-Holland

DECAY TIME AND LIGHT YIELD MEASUREMENTS FOR PLASTIC SCINTILLATING FIBERS

C.M. HAWKES, M. KUHLEN, B. MILLIKEN, R. STROYNOWSKI and E. WICKLUND
California Institute of Technology, Pasadena, CA 91125, USA

T. SHIMIZU and O. SHINJI
Kuraray Co. Ltd., Tokyo, Japan

Received 6 December 1989

We have studied light production and propagation in three different samples of plastic scintillating fibers manufactured by Kyowa Gas Co.: SCSF-81, SCSF-38 and SCSF-38 with a quenching additive. The emission time distribution is described phenomenologically by a fast two-step scintillation process and an additional slow component, the time constants of which are determined. The light yield from the fibers is measured as a function of distance for the two light components which propagate by total internal reflection from the core–clad interface and from the clad–air interface. We obtain the absolute light yield and attenuation lengths for the different fibers.

1. Introduction

Scintillating fibers are becoming widely used now in particle physics experiments. Various applications include charged particle tracking devices, active targets and calorimetry. It has been suggested recently to utilize the small inherent spread of the travel time for produced photons in scintillating fibers for time-of-flight measurements [1,2]. The absolute light yield and the attenuation characteristics of the fibers have an important impact on the design of the different detectors. In addition it is important to understand the timing characteristics of the fibers for applications such as time-of-flight measurements where short decay time and high light yield are desirable.

We have measured the light yield and the emission time distribution for 1 mm diameter round fibers produced by Kyowa Gas Chemical Industry Co. Ltd. *, with core material of the same composition as SCSN-38, SCSN-81, and SCSN-38 with 0.5% by weight of benzophenone added as a quencher (referred to as SCSN-38Q). The core of the fiber consists of doped polystyrene (index of refraction $n_1 = 1.59$) and the cladding is 0.03 mm polymethylmethacrylate (index of refraction $n_2 = 1.49$).

2. Light yield

In general, scintillating fibers consists of a core of scintillator material, with an index of refraction n_1,

* Now part of Kuraray Co. Ltd.

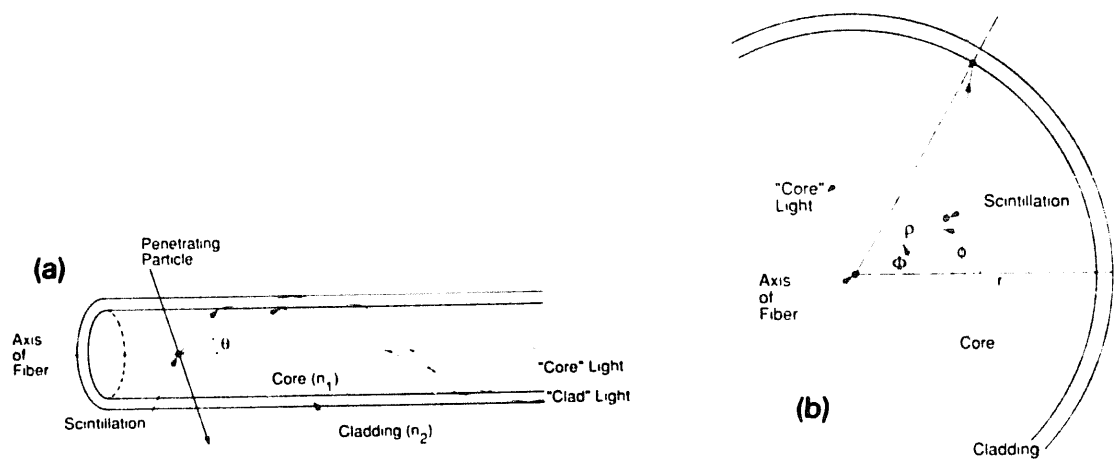

Fig. 1. Light propagation in a scintillating fiber for light rays emitted (a) on-axis and (b) off-axis.

0168-9002/90/$03.50

coated with a thin transparent cladding with a smaller index of refraction $n_2 < n_1$ (see fig. 1). The core–cladding interface provides a smooth surface for reflections.

For scintillation at a point on the axis of the fiber (fig. 1a) the generated light travels radially in the plane perpendicular to the fiber axis and so the angle of incidence at the reflecting surface is determined by just the polar angle θ. The light will be trapped by total internal reflection at the core–clad interface and propagate along the fiber ("core" light) if $\theta < \theta_{tr}$, where the trapping angle is the complement of the critical angle: $\cos\theta_{tr} = n_2/n_1$. Light not trapped in the core can be refracted into the cladding. This light will be trapped also by total internal reflection at the clad–air interface ("clad" light) if $\theta < \theta'_{tr}$ where $\cos\theta'_{tr} = 1/n_1$. Here θ is the initial polar angle of emission in the core, before refraction at the core–clad interface. For the round fibers used in our measurements the trapping angle does not represent a sharp cutoff. Scintillation light emitted away from the axis of the fiber (fig. 1b) has an angle of incidence with respect to the normal to the fiber surface which depends on both polar and azimuthal angles of emission. The condition for trapping by total internal reflection at the core–clad interface is

$$\sin\theta\sqrt{1-\left(\frac{\rho}{r}\sin(\phi-\Phi)\right)^2} < \sin\theta_{tr}, \qquad (1)$$

where (ρ, Φ) define the position of the point in the core at which the scintillation occurs, θ and ϕ are the polar and azimuthal angles of the direction of emission and r is the radius of the core (see fig. 1b). Hence some "core" light is trapped also for $\theta > \theta_{tr}$ when $\rho \neq 0$ and $\phi \neq \Phi$. A similar argument applies to the trapping of "clad" light. These off-axis light rays "spiral" along the fiber with a larger number of reflections and a longer path length than the on-axis rays and thus have a shorter attenuation length.

In general both "core" and "clad" light components are present and have been observed. The relative contribution of each component depends on the attenuation length and on the measurement method. Due to external surface imperfections we expect the light reflecting off the clad–air interface to have much shorter attenuation length than the light reflecting off the core–clad interface.

2.1. Experimental setup

The setup for measuring the light yield of scintillating fibers is shown in fig. 2. A single 2.50 m long, 1 mm diameter fiber is held straight in a steel tube that maintains the position of the fiber relative to a beam of electrons from a collimated ^{106}Ru source. The source emits electrons with a maximum energy of 3.5 MeV. The beam penetrates the steel tube through holes and

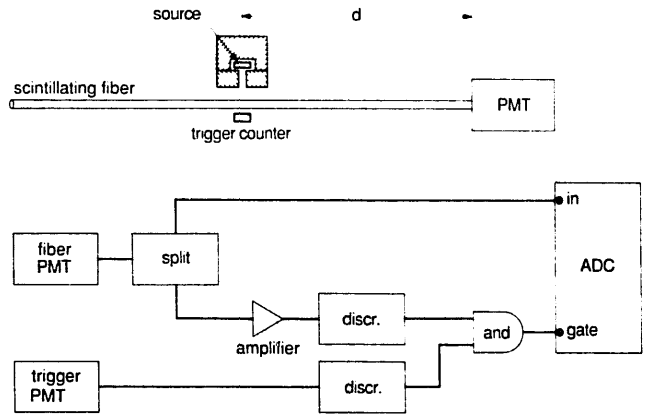

Fig. 2. Block diagram of setup for light yield measurement.

represents a roughly uniform distribution of parallel tracks across the width of the fiber.

The end of the fiber is cast into a disk of optical glue (see fig. 3) with index of refraction n_3 close to the one of the fiber core (glue: $n_3 = 1.57$, core: $n_1 = 1.59$). The "core" light stays trapped inside the fiber, while the "clad" light is coupled into the transparent disk and refracted away from the fiber axis, resulting in spatial separation of the two components. The "clad" light will leave the fiber with angles θ in the range $\theta_1 < \theta < \theta_2$ and illuminate a ring on the disk's surface. The limiting angles are given by $\cos\theta_1 = n_2/n_3$ and $\cos\theta_2 = 1/n_3$. Rays emitted off-axis which have "spiraled" down the fiber may emerge at larger angles than θ_2 and blur the outer boundary. The two light components can then be

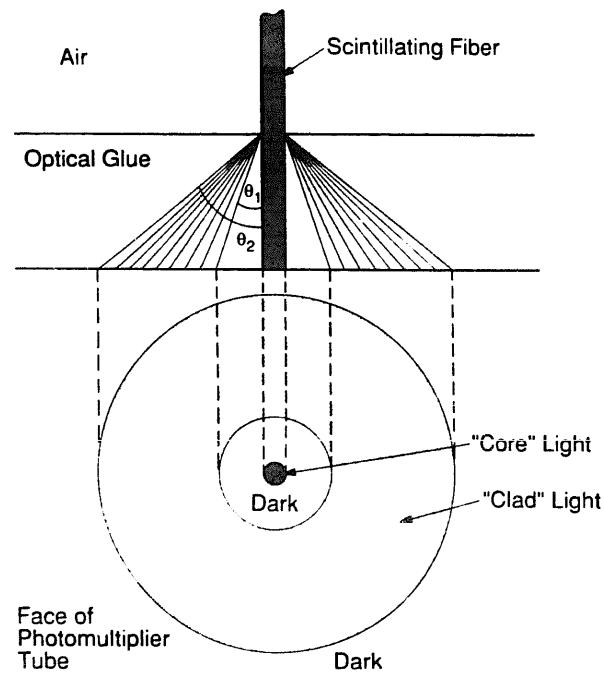

Fig. 3. Simplified sketch of the "core" and "clad" light separation. "Clad" light emission into the glue may occur over an extended distance along the fiber.

separated using opaque masks. The light emerging from the polished disk/fiber face is coupled to an Amperex XP2020 photomultiplier tube with an elastic Sylguard "cookie" [3].

The charge from the photomultiplier is measured with a LeCroy 2249W ADC which is gated by the coincidence of signals from a trigger counter placed behind the scintillating fiber and from the fiber itself. The extra requirement of a signal from the fiber is used to reject events that would have been otherwise triggered by the dark current of the trigger counter. To prevent this requirement from distorting the pulse charge distribution we cascade three ORTEC 574 low-noise wideband amplifiers and use a low discrimination threshold – well below the single photoelectron level – to form the input to the coincidence gate from the fiber. Light yield measurements made without this coincidence agree with results for which the coincidence had been required. Fig. 4 shows a typical pulse charge distribution. Once can clearly distinguish the separate peaks due to one- and two-photoelectron events.

2.2. Data analysis

It is assumed that for fixed charged track path length in the scintillator the number of photoelectrons detected follows a Poisson distribution. The distribution of charged track path lengths in the round fiber is calculated assuming a uniform illumination across the fiber and that all tracks are parallel. The path length distribution for the round fiber is convoluted with the Poissonian photoelectron distribution to form a probability function $P(n;\ \mu,\ r)$ for the number of detected photoelectrons n,

$$P(n;\ \mu,\ r) = \int_0^r \frac{x/r}{\sqrt{r^2 - x^2}} \frac{e^{-2\mu x}(2\mu x)^n}{n!} dx. \qquad (2)$$

Here μ is the mean number of detected photoelectrons per unit track length in the fiber, and r is the radius of the scintillating fiber. The non-Gaussian shape of the response of the photomultiplier tube to single-photoelectron events [4] makes it difficult to describe the spectra by an analytical function. Instead, the phototube's response to incoming photons is modeled by a Monte Carlo procedure, which uses the measured response for single-photoelectron events as input. Fig. 5 shows the measured ADC spectrum for single-photoelectron events obtained by filtering the light down to a level of roughly 0.05 photoelectrons on average. We observe a single-photoelectron peak at about 30 ADC counts above the pedestal, and a nonvanishing valley between the peak and the pedestal. The response for events with multiple photoelectrons is calculated by adding pulse charges which have been chosen from the single-photoelectron distribution according to its measured probability distribution. The data can be well described by this procedure (see fig. 4), and a relationship between the mean of the ADC distribution and the underlying variable μ can be established. Using this relationship, we convert observed means of the ADC spectra into the mean number of detected photoelectrons per unit path length, μ.

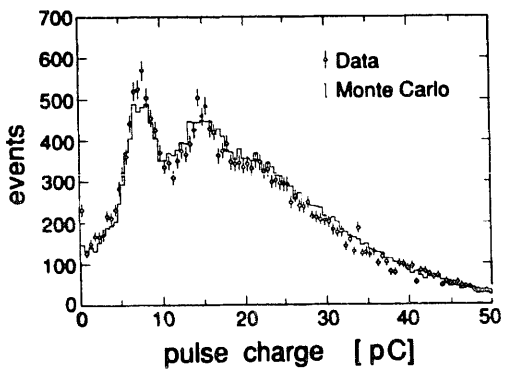

Fig. 4. Pulse charge distribution for light yield measurement. The points represent the data. The histogram is a Monte Carlo simulation for a mean number of photoelectrons of 4.02 per mm of scintillator which represents the best fit to the data.

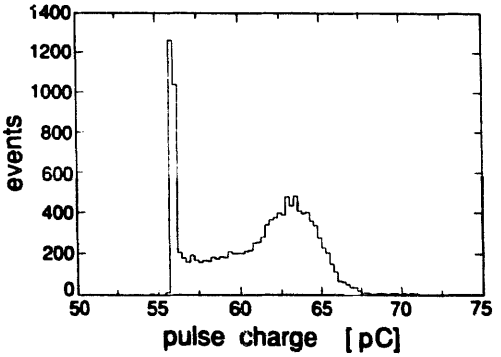

Fig. 5. Pulse charge distribution for single-photoelectron events.

For distances close to the phototube ($\leqslant 0.3$ m) with large light level we observe an enhanced number of single-photoelectron events, which cannot be accounted for by the Poisson statistics of the above model. We conclude that there is a weak statistically independent light source contributing at short distances. The effect is most prominent in the "clad" light. The region of the one-photoelectron peak is excluded from the analysis for light levels corresponding to more than eight photoelectrons.

2.3. System performance

Possible misalignment of the source, variation in optical coupling, and variation in photocathode sensitivity are found to affect the results by less than 5%. Repeated glueings gave maximal deviations in the light measurement of 13% at short distances ($\leqslant 0.3$ m) and

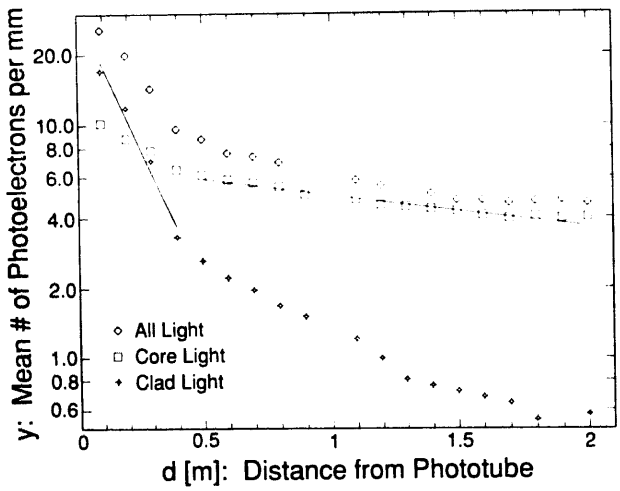

Fig. 6. Light yield as a function of distance for SCSF-81.

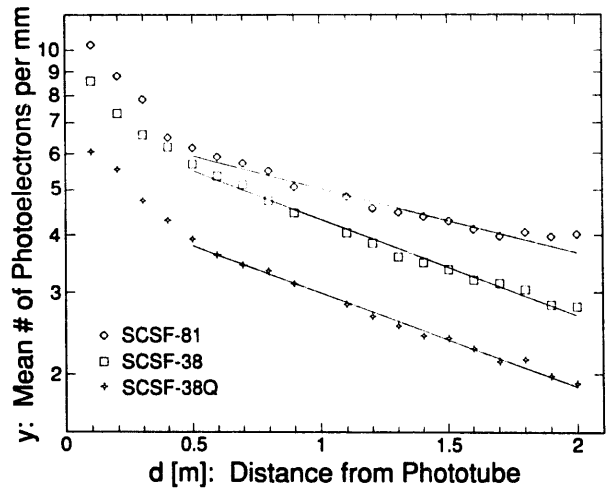

Fig. 7. "Core" light yield as a function of distance for different scintillators.

5% at long distances ($\geq$ 1.3 m). As a test of the linearity of our measurement procedure and our ability to separate the "core" and the "clad" light we compare the sums of the individual core and clad measurements at each point with a measurement of the total light without masks. On average they agree to within 3%. We have also performed a core light measurement with about 3 cm of the fiber end which goes into the glue disk painted black to absorb all "clad" light contributions. This measurement agrees with the measurement where the "clad" light has been masked out.

2.4. Light yield results

The dependence of the light yield on the distance d from the phototube is shown in fig. 6 for the "core" light, the "clad" light and the measured sum of both types for a fiber SCSF-81. We fit a single exponential function

$$y = y_0 \, e^{-d/\lambda} \qquad (3)$$

to the data, where y is the mean number of detected photoelectrons per mm of path length in the scintillator and λ is the attenuation length. The "core" light has a long attenuation length $\lambda = 3.3$ m for large distances (0.5 m $\leq d \leq$ 2.0 m) while the "clad" light, which dominates at short distances, is attenuated much faster over the first few points ($\lambda = 0.18$ m for 0.1 m $\leq d \leq$ 0.4 m).

This behavior can be explained by a very good core-clad interface giving rise to a long "core" light attenuation length and by the imperfections at the clad-air interface, which attenuate the "clad" light much faster. For the present choice of the indices of refraction of the core and cladding the "clad" light has a larger geometrical trapping acceptance than the "core" light. Thus the clad contribution exceeds the core contribution at short distances. At larger distances it is attenuated below the "core" light level. The observation that the "clad" light does not follow a smooth attenuation curve indicates a nonuniform surface quality of the fiber.

The "core" light also exhibits a steeper attenuation at short distances. That effect may be partly due to the "spiraling" contribution from off-axis photon emission, partly due to the shorter attenuation length of the short wavelength component and the self-absorption by the final wavelength shifter, and partly due to "clad" light feeding into the "core" light. In the same way the shallower attenuation of the "clad" light at larger distances may be explained by regeneration from the "core" light. It should be noted that while we were able to reproduce the "core" light measurements after repeated handling of the fiber sample, the "clad" light output degraded each time. We attribute this effect to damage done to the exposed clad surface.

We now compare the three fibers made of scintillators with different chemical compositions: SCSF-81, SCSF-38 and SCSF-38Q. The results of the "core" light measurements are shown in fig. 7. The measurements are not affected by the variations in the surface quality of the fibers. The data for distances $d \geq 0.5$ m can be described by an exponential attenuation law (eq. (3)). The results of the fits to the data are given in table 1. The errors are derived from the rms deviation of the individual points from the fitted curve.

Table 1
Light yield and attenuation in fiber core

Scintillator	y_0 [p.e./mm]	Attenuation length λ [m]
SCSF-81	6.84 ± 0.17	3.32 ± 0.21
SCSF-38	6.93 ± 0.14	2.12 ± 0.07
SCSF-38Q	4.74 ± 0.07	2.18 ± 0.05

For distances greater than 0.1 m the SCSF-81 fiber has highest light output and also has longest attenuation length. Adding the quencher to SCSF-38 results in a reduction of the light output by roughly a third, while the attenuation length is not altered.

3. Emission time distribution

The details of the scintillation process are discussed in depth by Birks [5] and have recently been reviewed [6,7]. Many processes contribute to the emission of scintillation light. The emission time distribution in plastic scintillators can be described as consisting of a fast component generated by a two-step scintillation cascade and a slow component that can be approximated by a single-step process. The expected emission time probability distribution with this assumption is

$$E(t) = \frac{\dfrac{e^{-t/\tau_2} - e^{-t/\tau_1}}{\tau_2 - \tau_1} + \dfrac{R}{\tau_3} e^{-t/\tau_3}}{1 + R}, \qquad (4)$$

where τ_1 and τ_2 are the decay constants of the fast two-step scintillation process, τ_3 is the decay time of the slow component and R is the ratio of the light components produced through the slow and fast decay processes. The short-time behavior is dominated by the rise and decay time generated by the two-step cascade. The addition of a quencher opens another decay channel for the scintillating state, thus shortening its lifetime at the cost of the yield of scintillation light.

3.1. Experimental setup

The emission time distribution of the scintillator is measured using a time correlated single-photon counting technique. Fig. 8 shows the setup. The scintillator is excited by electrons from a ^{106}Ru source. The decay

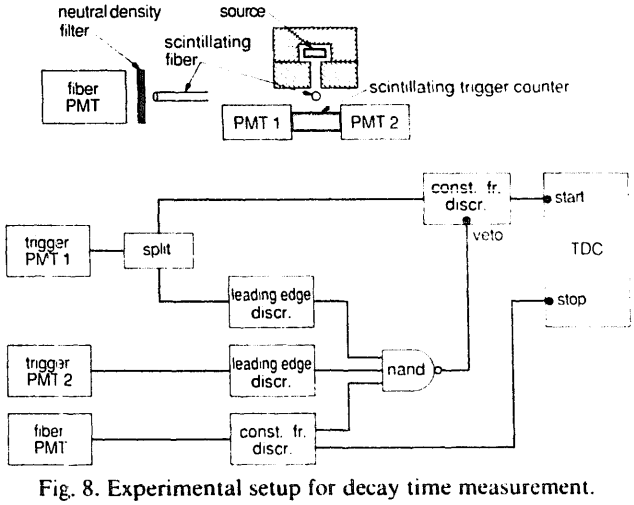

Fig. 8. Experimental setup for decay time measurement.

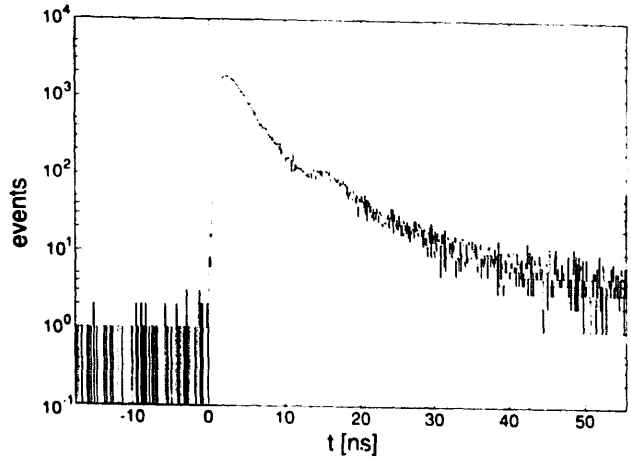

Fig. 9. Time distribution for a decay time measurement.

photons are detected by an Amperex XP2020 phototube which is coupled to the scintillating fiber through a neutral density filter. The filter reduced the detected signal to an average of approximately 0.05 photoelectrons. After leaving the fiber the electron from the source enters a 2 cm deep block of scintillator which is coupled to XP2020 phototubes on each end. The signals from these two phototubes are used both to select the events of interest and to measure the time at which the electron traversed the system. Because the thick scintillator results in a large number of photoelectrons it provides a precise measurement of the traversal time. The minimum number of photoelectrons required to satisfy the event discriminators is about 100 and the mean number of photoelectrons is about 300. The signal from one of the two event selection phototubes is split and discriminated using an ORTEC 934 constant-fraction discriminator. The discriminator output is used to start a LeCroy 2228A TDC. The signal from the fiber sample phototube is also discriminated with a constant-fraction discriminator and the output is used to stop the TDC. The threshold on the start discriminator is set at roughly the three-photoelectron level to optimize the time resolution of the start.

An example of the TDC distribution measured with this system is shown in fig. 9. One sees the expected fast rise of the distribution, attributable both to the rise time of the scintillator and to the transit time spread of the phototube. There are three dominant features on the falling side of the distribution: the fast component dominating the first 10 ns, the slow component and a broad second peak occurring roughly 13 ns after earliest emission times.

The system response has been studied by replacing the scintillating fiber with a piece of lucite which yields fast Cherenkov light signals (see appendix A). These studies suggest that the peak at 13 ns is due to an afterpulsing of the phototube.

3.2. Data analysis

The data have been fitted to the hypothesis that the measured time distribution is the convolution of the emission time distribution $E(t)$ (eq. (4)) and the system resolution function. The resolution function may be approximated by a Gaussian distribution with standard deviation fixed at $\sigma_t = 280$ ps, the value obtained using Cherenkov light. The resulting distribution

$$P(t) = \int_0^\infty E(t') \frac{1}{\sqrt{2\pi}\sigma_t} e^{-(t-t')^2/2\sigma_t^2} dt'$$
$$= \frac{1}{1+R}\left[\frac{\tau_2 f(t, \tau_2) - \tau_1 f(t, \tau_1)}{\tau_2 - \tau_1} + R f(t, \tau_3)\right], \quad (5)$$

where

$$f(t, \tau) \equiv \int_0^\infty \frac{1}{\sqrt{2\pi}\sigma_t} e^{-(t-t')^2/2\sigma_t^2} \frac{1}{\tau} e^{-t'/\tau} dt'$$
$$= \frac{1}{2\tau}\left[1 + \mathrm{erf}\left(\frac{1}{\sqrt{2}}\left(\frac{t}{\sigma_t} - \frac{\sigma_t}{\tau}\right)\right)\right] e^{-(t/\tau - \sigma_t^2/2\tau^2)}, \quad (6)$$

is used to perform a maximum likelihood fit to estimate the parameters τ_1, τ_2, τ_3, and R.

The range over which afterpulsing distorts the time distribution has been determined also from Cherenkov light studies. As a result, the data between 11.5 and 20.8 ns have been excluded from the likelihood analysis. Because of the small probability of emission from the scintillator tens of nanoseconds after the earliest emissions and because of the small but finite probability of dark current coincidences the total range of data included in the analysis is limited to the first 35 ns. An example of a measured TDC distribution with the fit result is shown in fig. 10.

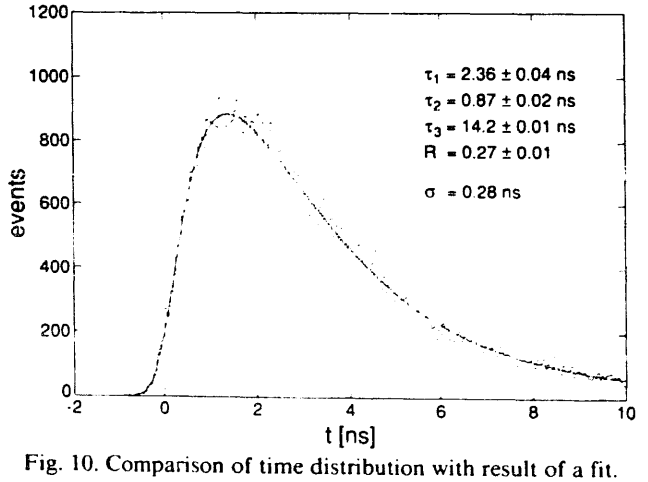

Fig. 10. Comparison of time distribution with result of a fit.

Table 2
Measured parameters of emission time distribution

Scintillator	Rise time τ_1 [ns]	Decay time τ_2 [ns]	Slow comp. τ_3 [ns]	Ratio slow/fast R
SCSN-81	0.87±0.02	2.36±0.04	14.2±0.4	0.27±0.01
SCSN-38	0.68±0.02	2.27±0.05	14.9±0.4	0.25±0.01
SCSN-38Q	0.71±0.03	2.08±0.06	14.9±0.5	0.21±0.02

3.3. System performance

The timing characteristics of the system have been studied using calibrated delay cables. The delay cables were calibrated using an HP 5370B time interval counter which provided a precision of 4.8% in the absolute time scale and an accuracy of 0.2% in the relative length of the cables. The system was linear to 0.3% over 10 ns.

The reproducibility of the data and of the analysis results have been tested by repeated measurements with a single scintillating fiber. The errors obtained from the fitting procedure for a single measurement were found to be consistent with the spread of fit results from the independent measurements.

Systematic uncertainties arising from sensitivity to the choice of the range of data included in the analysis have been investigated. For reasonable changes in these ranges the changes in the parameter values are less than or equal to the statistical errors.

3.4. Emission time results

The parameter values found for the three scintillators along with statistical errors are shown in table 2. The relative speed of the scintillators can be judged by considering the integral of the normalized emission time distribution from 0 to t. Using the parameter values from table 2 and eq. (4) this integral representation is

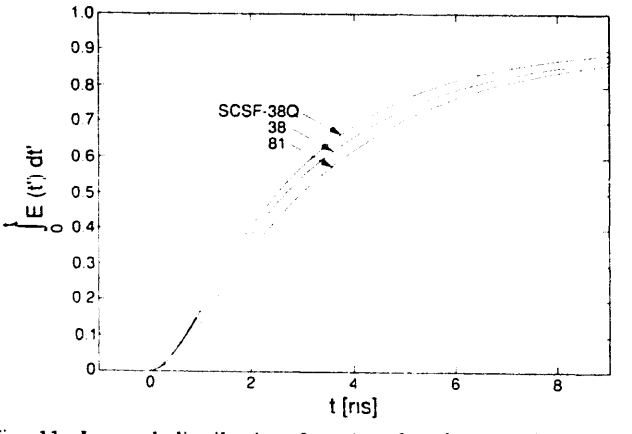

Fig. 11. Integral distribution function for the emission time distribution.

shown in fig. 11. The SCSN-38 scintillator has a faster emission time than the SCSN-81 scintillator. The addition of a quencher component to SCSN-38 results in increased speed of the decay time of the SCSN-38Q scintillator.

4. Conclusion

We have measured the characteristics of several scintillating fibers. Light propagating by total internal reflections from the core–clad interface and from the clad–air interface have clearly been distinguished. Due to an imperfect clad surface, the "clad" light dies out very quickly, while the "core" light has a long attenuation length.

For particle detector applications the presence of the "clad" light is sometimes not needed or even unwanted. Its propagation depends on the surface quality of the fiber which is hard to control, and it may lead to cross talk between neighboring fibers. Extramural absorbers applied to the fiber surface may be necessary for particular applications.

There are significant differences in the light yield and some differences in the decay times of the scintillators considered. In particular, addition of a quencher to SCSN-38 results in increased speed of the decay process at the expense of reduced light yield. For TOF applications, however, a slight increase in speed does not seem to justify the sacrifice of a third of the light output.

Acknowledgements

The authors wish to thank C. Peck and F. Porter for their valuable suggestions and insights. Special thanks are due to S. Sondergaard for his technical assistance. One of us (M.K.) acknowledges the Alexander von Humboldt Foundation for its support. This work was funded in part by the U.S. Department of Energy under contract no. DE-AC03-81ER40050.

Appendix A

Cherenkov light studies

To understand the system response function the scintillating fiber sample was replaced by a 2 cm thick disk of lucite. Cherenkov light produced by the passage of electrons from a ^{106}Ru source was used to generate the TDC stop. Since the light from the Cherenkov process is emitted essentially instantaneously and since the light output was limited to a single photoelectron for this study, the measured time distribution is a direct measure of the system response. The time response of the photomultiplier tube is known to depend on the position at which the light impinges on the photocathode. Therefore the entire surface of the lucite disk was painted black except for a 2 mm diameter hole pointing to the center of the photocathode. This is the region of the photocathode to which the fiber was coupled in the studies using scintillation light. Fig. 12 shows a typical Cherenkov time distribution. As with the time distribution measured using scintillation light ones sees two distinct peaks, with the second peak contributing less than 1% to the total signal.

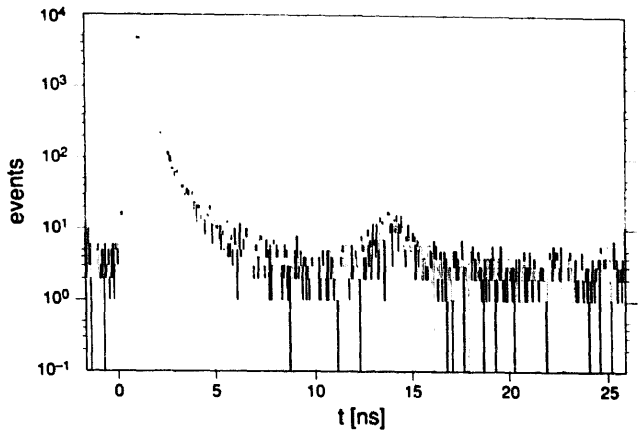

Fig. 12. System response measurement with Cherenkov light.

The system resolution was estimated by measuring the full width at half maximum of the distribution. It is interesting to note that the response is not Gaussian - the leading edge of the distribution is sharper than the

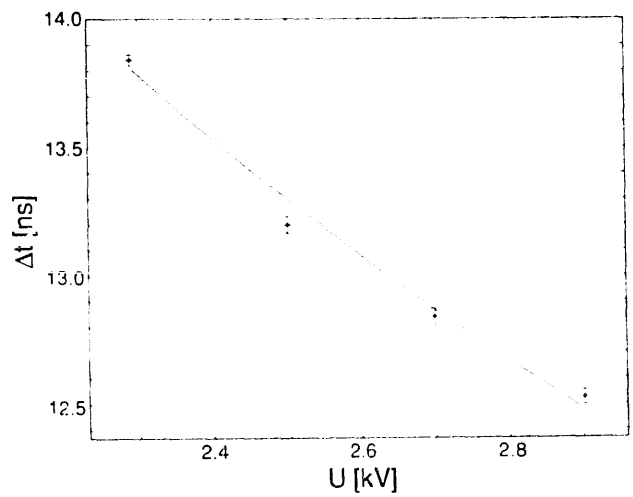

Fig. 13. Dependence of the second peak position on the high voltage.

trailing edge. The convolution of a Gaussian and an exponential,

$$P(t-t_0)=\frac{1}{2\tau}\left(1+\mathrm{erf}\left[\frac{1}{\sqrt{2}}\left(\frac{t-t_0}{\sigma}-\frac{\sigma}{\tau}\right)\right]\right)\times\exp\left[-\left(\frac{t-t_0}{\tau}-\frac{\sigma^2}{2\tau^2}\right)\right], \quad (7)$$

fits the shape of the distribution reasonably well with a resolution of $\sigma = 190$ ps and a decay constant of $\tau = 390$ ps. The data are shown in fig. 12. In the Gaussian approximation the measured system resolution is 280 ps.

To study the possibility that the second peak is due to afterpulsing several sets of data were generated with the phototube voltages ranging between 2290 and 2900 V. The first peak for each measurement is fitted to eq. (7) in order to find t_0. The second peak is well described by a Gaussian distribution and is fit to find the Gaussian mean t_0'. The time difference $\Delta t = t_0 - t_0'$ is shown in fig. 13 as a function of the phototube voltage. If the second peak is generated by photons liberated at the first dynode that return to the photocathode and there produce additional electrons then one would expect that this time difference would decrease as the tube voltage is increased. In particular if the acceleration of the photoelectron can be approximated as constant one would expect the time difference to depend on the voltage as

$$\Delta t = \frac{\sqrt{v_0^2 + aU} - v_0}{bU}, \quad (8)$$

where U is the tube voltage, and a, b, and v_0 depend on the electric field characteristics of the tube, the distance from the photocathode to the dynode, the distribution of electron velocities at the photocathode, and on the mass and charge of the electron. As fig. 13 shows, this function describes the data only approximately. Presumably, the precise form of the voltage dependence of the time difference is a more complicated function of the electric field characteristics of the tube. A similar observation of afterpulsing is described in ref. [8].

References

[1] B. Milliken, R. Stroynowski and E. Wicklund, Caltech preprint CALT-68-1538 (1989); Proc Workshop on Scintillating Fiber Detector Development for the SSC, Fermilab (Nov. 1988) p. 313.

[2] M. Kuhlen, Caltech preprint CALT-68-1547 (1989); Proc. of the Int. Industrial Symp. on the Super Collider, New Orleans (Feb. 1989), ed. M. McAshan, p. 611.

[3] Sylguard 184 resin and curing agent mixed with Dow Corning 200 Electronic Fluid with the viscosity of 20×10^{-2} stokes.

[4] Philips Data Handbook for Electron Tubes T9 (1987).

[5] J.B. Birks, The Theory and Practice of Scintillation Counting (Oxford, 1964).

[6] A Grimes et al, Northeastern University preprint NUB-2943 (1988).

[7] J. Flournoy, Proc. Workshop on Scintillating Fiber Detector Development for the SSC, Fermilab (Nov. 1988) p. 505.

[8] S.S. Stevens and J. Longworth, IEEE Trans. Nucl. Sci. NS-19 (1972) 356.